inorganics

MDPI

Article

Sustainable Semicrystalline/Nanocrystalline UiO-66-Type Zr-MOFs as Photodegraders of Rhodamine B

Jemal M. Yassin [1,*], Abi M. Taddesse [2] and Manuel Sánchez-Sánchez [3,*]

[1] Department of Chemistry, Debre Berhan University, Debre Berhan P.O. Box 445, Ethiopia
[2] Department of Chemistry, Haramaya University, Dire Dawa P.O. Box 138, Ethiopia; abi92003@yahoo.com or abi.taddesse@haramaya.edu.et
[3] Institute of Catalysis and Petroleum Chemistry (ICP), CSIC, 28049 Madrid, Spain
* Correspondence: jemalchemistry@gmail.com or jemalmohammed@dbu.edu.et (J.M.Y.); manuel.sanchez@icp.csic.es (M.S.-S.); Tel.: +251-912867429 (J.M.Y.); +34-915119711 (M.S.-S.)

Abstract: UiO-type Zr-BDC MOFs have garnered the interest of the scientific community due to their exceptional diversity in composition, structure, and chemical environment, as well as their high thermal and chemical stabilities. This work demonstrates the sustainable synthesis of a series of nanocrystalline/semicrystalline UiO-66(Zr) metal–organic frameworks (MOFs) under facile conditions—specifically at room temperature, in water, with high yield, and without the use of modulators or toxic byproducts. The synthesis involves either deprotonating the linker or utilizing various ratios of water and DMF as solvents. The as-prepared materials obtained from both synthesis strategies share key structural features with conventional UiO-66(Zr) in their short- and medium-range physicochemical properties, while exhibiting significant differences in crystallinity and textural properties. Nonetheless, the materials generally lack long-range order (semicrystalline), in particular these synthesized following the deprotonation strategy. However, the materials prepared using mixed solvent strategy seem to exhibit characteristics of nanocrystalline UiO-66(Zr). Overall, both approaches successfully addressed various synthesis challenges related to the highly sought-after Zr-based metal–organic frameworks (MOFs). Some of these MOF materials were tested for the photodegradation of rhodamine B (RhB) under mercury light irradiation, evidencing high photocatalytic efficiency of up to 75 ± 0.078% within 120 min under the pseudo-first-order model. This suggests an interaction between the photocatalyst and the RhB dye, involving electron injection from RhB and the ability for ligand-to-metal charge transfer (LMCT), which enhances the efficient photocatalytic degradation of RhB. The trapping experiments indicated that superoxide radicals ($\bullet O_2^-$) and photogenerated holes (h^+) are crucial in the photodegradation of RhB. Moreover, the materials showed good recyclability across five tested cycles. A plausible photocatalytic reaction mechanism has been proposed to explain these findings.

Keywords: sustainable synthesis; UiO-66-type MOFs; RhB degradation; semicrystalline; nanocrystalline

check for updates

Academic Editors: Torben R. Jensen, Chao-Ming Huang and Guan-Ting Pan

Received: 5 February 2025
Revised: 9 April 2025
Accepted: 20 April 2025
Published: 24 April 2025

Citation: Yassin, J.M.; Taddesse, A.M.; Sánchez-Sánchez, M. Sustainable Semicrystalline/Nanocrystalline UiO-66-Type Zr-MOFs as Photodegraders of Rhodamine B. *Inorganics* **2025**, *13*, 131. https://doi.org/10.3390/inorganics13050131

Copyright: © 2025 by the authors. Licensee MDPI, Basel, Switzerland. This article is an open access article distributed under the terms and conditions of the Creative Commons Attribution (CC BY) license (https://creativecommons.org/licenses/by/4.0/).

1. Introduction

UiO-66(Zr) MOFs are amongst the most well-known and considerably researched nanoporous materials. Compared to other MOFs, they are favored for their relatively high thermal stability (above 500 °C), chemical and mechanical resilience, low toxicity, and the high abundance of their constituent materials. UiO-66(Zr) is made up of $[Zr_6O_4(OH)_4]^{12+}$ clusters and terephthalate $[BDC]^{2-}$ linkers that act as inorganic nodes and organic spacers,

respectively. Commonly, they are prepared via a solvothermal approach using expensive and unsafe solvents at high temperature [1]. The strong coordination in the framework prevents the attack of guest molecules, like water, maintaining the intact crystal structure [2,3]. Hence, these types of MOFs are desired for a range of potential applications, such as heterogeneous (photo)catalysis, gas storage and separation, sensing, etc. [4–8].

Nevertheless, their practical applications have been inhibited by the high costs associated with synthesis conditions. These include the necessity for elevated temperatures, prolonged reaction times, relatively expensive zirconium precursors, the use of non-aqueous solvents, and specific amounts and types of modulators. These factors render large-scale industrial production unsustainable and have hindered breakthrough applications [4,9–13]. To date, the use of modulators, functionalized linkers, and/or structure-directing agents/templates to prepare UiO-66(Zr) in aqueous solution at room temperature has proven to be strategic. This approach enhances the reproducibility and crystallinity of the materials while allowing for control over the particle size and defect density in the resulting framework, all without compromising structural integrity [14–18]. Furthermore, certain research groups have attempted the effective design and synthesis of UiO-66(Zr) under mild conditions through various strategies, such as (i) by careful selection of Zr precursors (namely, chloride, oxychloride octahydrate, oxynitrate, acetate solution, sulphate, acetylacetonates, methacrylate oxo-cluster, etc.) [14,19–22]; (ii) by using different modulators (benzoic acid, formic acid, trifluoroacetic acid, acetic acid, etc.), which have the same chemical functionalities (carboxylate groups) as terephthalate [12,17,23–25]; (iii) by using functionalized linkers (-NH_2, -F_4, etc.) [24,26–28]; (iv) by changing the organic linkers (for instance, using H_4BTC/H_3BTC instead of H_2BDC) [26]; (v) by adding a structural directing agent or template or salting-in-species during pre- and post-synthesis [29–31]; and (vi) by applying other different synthesis approaches [13,14,30,32,33].

Materials synthesis at room temperature is more sustainable and even more effective than the common well-known methods, at least for certain applications [12,20,34]. Nevertheless, sustainable synthesis of UiO-66(Zr) in aqueous or less toxic media without modulator, structural directing agent, template, or salt effects, and without energy input, remains a great challenge [13,35,36]. Such methodologies are still scarce and require further exploration, primarily due to the poor solubility of terephthalic acid in water at room temperature (only 0.0015 g/100 mL at 20 °C) and the aforementioned challenges.

In light of the above, one of the aims of this work was to synthesize UiO-type Zr-BDC MOFs at room temperature using various Zr precursors, employing different synthesis strategies developed in our research group [10,35,37–39]. Semicrystalline UiO-type Zr-BDC and nanosized UiO-66(Zr) MOFs were successfully synthesized using Zr oxychloride, Zr oxynitrate, Zr acetate solution, and Zr chloride at room temperature through the following two systematic approaches: (1) utilizing water as the sole solvent in the presence of NaOH as a deprotonating agent, without any modulator, pH adjustment, or other additives; and (2) using different molar ratios of water and DMF (N,N-dimethylformamide) as the reaction medium. The later approach is less sustainable due to the involvement of DMF, which was necessary to ensure the solubility of the linker. In both approaches, different Zr precursors were tested. The main role of NaOH in the former approach is to improve both the solubility and the deprotonation of terephthalic acid. In addition, these strategies aim to create a more sustainable system by reducing the corrosiveness associated with the formation of harmful byproducts, such as HCl and HNO_3, in the synthesis media [10]. Ultimately, these novel and systematic synthesis approaches are designed to meet the critical 3E (environmental, energetic, and economic) requirements [10,12,18,35,38–42] for effective industrial implementation.

In the early 2000s, metal–organic frameworks (MOFs) were proposed as potential photocatalysts due to their semiconductor properties [43–45]. They can be activated through irradiation, transferring photogenerated electrons from the organic linker—acting as an antenna—to the vacant d-orbitals of the metal cluster via a mechanism known as ligand-to-metal charge transfer (LMCT) [44,46–48]. However, pristine semicrystalline Zr-BDC or UiO-66(Zr) MOFs exhibited poor photocatalytic activity under visible light irradiation, similar to other wide band gap semiconductors. This limitation arises from the optical properties of Zr-oxo clusters, which only absorb UV light, and the rapid recombination rate of charge carriers [35,49,50]. To overcome these challenges, one approach involves preparing composites of Zr-based MOFs with specific semiconductors that can address these deficiencies [35,41,42,51,52]. Alternatively, conducting photocatalytic experiments under UV or mercury light irradiation can enhance photocatalytic performance. This work explores the latter approach in the degradation of rhodamine B (RhB) dye, which possesses a high charge transfer capability [53,54]. Our results demonstrate the very good photocatalytic performance of Zr-based MOFs synthesized through different sustainable methods.

2. Results

2.1. Characterization of the MOF Materials

The intensity-normalized background-removed PXRD patterns of different Zr-BDC MOFs prepared via different strategies from different Zr precursors are depicted in Figure 1. The samples prepared in the presence of NaOH as deprotonating agent were called with the name of the anion precursor that is, Oxychloride, Oxynitrate or Acetate, whereas the samples prepared from mixture of solvents media were denoted as Precursor-r, where r stands for the water/DMF molar ratio (Table S1), which was 3, 1, or 0.33. Figure S1a shows the as-registered XRD patterns (that is, before background removal) of the samples whose XRD patterns are shown in Figure 1. All diffractograms of the samples prepared under sustainable conditions have certain features in common regardless the synthesis strategy or the Zr precursor used. In particular, the major diffraction peak is observed at 2θ values of approximately 7.4° in all cases, which aligns closely with the XRD pattern of the Nano-UiO-66(Zr) MOF synthesized via the conventional solvothermal approach at 120 °C. This consistent peak indicates that the synthesized material is indeed a nanocrystalline UiO-66(Zr). This conclusion is supported by comparisons with the experimental XRD pattern of commercial UiO-66(Zr) [35] and the simulated XRD pattern of UiO-66(Zr) (see Figure 1). The strategy using NaOH as the deprotonating agent provokes the immediate formation of a white precipitate as soon as the metal and linker solutions are mixed. Figure S1b shows the XRD patterns of the Zr-BDC samples prepared with Zr-oxynitrate when collected after 30 min, 2 h, 24 h, and 48 h, indicating that the sample is already formed and possesses practically the same XRD pattern with a very short synthesis time. The use of the Zr acetate precursor produces samples with broader peaks in their diffraction patterns (Figure 1a). Therefore, the samples achieved through this approach are semicrystalline UiO-type Zr-BDC MOFs, exhibiting key structural features with conventional UiO-66(Zr) in their short- to medium-range order with disordered regions but lacking long-range order. Nonetheless, these MOF materials exhibited significant differences in crystallinity and textural properties. Affording sustainably prepared UiO-66(Zr) MOFs with improved crystallinity presumably requires different synthetic approaches, since there have been few investigations on Zr-based MOFs at room temperature.

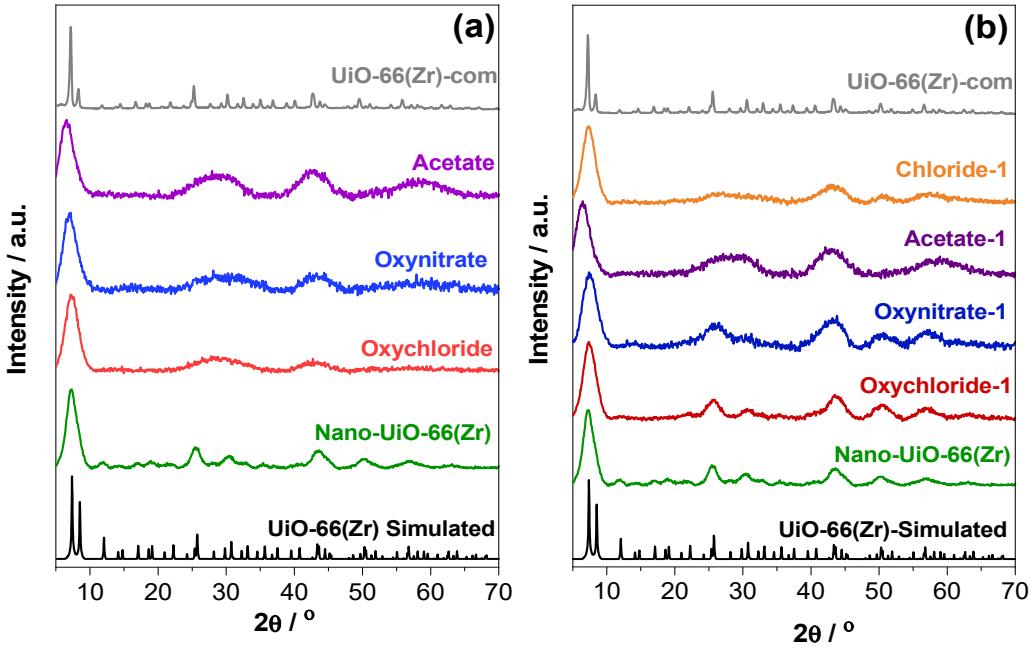


Figure 1. Intensity-normalized background-removed PXRD patterns of sustainably synthesized UiO-type Zr-BDC samples achieved starting from different Zr precursors and by different strategies: (**a**) by deprotonating the linker with NaOH; (**b**) by using a mixture of solvents, H_2O and DMF, with a molar ratio of 1. For comparison purposes, the simulated XRD patterns of UiO-66(Zr), the experimental XRD patterns of nanocrystalline UiO-66(Zr) (Nano-UiO-66(Zr)), and commercial UiO-66(Zr), are also shown. The as-registered XRD patterns are shown in Figure S1.

In this context, the driving force for our second sustainable synthesis approach is to combat the very low solubility of the linker H_2BDC in the synthesis media. Partially sacrificing the sustainability of the process, this strategy includes the use of DMF as a co-solvent of water, taking advantage of its high capability to dissolve terephthalic acid. Thus, nanocrystalline (the crystalline domains being extremely small) UiO-66(Zr) MOFs were synthesized at room temperature at different water/DMF ratios (Table S1) using various Zr precursors and the diprotic linker (H_2BDC) in the absence of any additive (such as a deprotonating agent or modulators). In general terms, the PXRD patterns of the MOFs obtained using these solvent mixtures (Figure 1b) did indeed exhibit relatively better crystallinity for all metal precursors compared with the samples prepared in water as the sole solvent (Figure 1a). In addition, the equimolar mixture of solvents showed slightly better crystallinity compared with their counterparts (Figure S2). On the other hand, we have noticed certain differences in the results obtained depending on the metal source. For example, Zr oxychloride and Zr oxynitrate precursors were suitable for the formation of nanosized UiO-66(Zr) at all water/DMF ratios (Figure S2a,b), whereas Zr acetate solution yielded UiO-66(Zr), the XRD pattern of which contains more broad diffraction peaks (Figure 1) probably due to an even more reduced (semi)crystallinity. In contrast, Zr-chloride produced the required MOF material only at an equimolar water/DMF ratio (Figure 1b and Table S1), and its PXRD shows a broader reflection.

However, the resulting precipitate obtained through the mixture of solvents strategy required a much longer reaction time (from 24 h to 96 h, depending on the amount of DMF) than the MOFs obtained using water as the sole solvent, which were formed instantaneously (Figure S1b).

For comparison, UiO-66(Zr) was prepared using a solvothermal approach with zirconium oxychloride octahydrate in DMF as a solvent at 120 °C for 24 h (the Nano-UiO-66(Zr) sample). This synthesis method, as described elsewhere [35], led to a sample whose diffrac-

tion pattern is not so different to that of the UiO-66(Zr) obtained at room temperature (Figure 1b). This similarity in diffraction patterns suggests that both synthesis methods yield comparable structural features for the UiO-66(Zr) materials. The effect of synthesis approach, reaction media, and the source of metal precursors in attaining better crystalline MOFs is evidenced by the relatively good matching of their XRD patterns with that of the commercial or simulated UiO-66(Zr). From the results depicted in Figures 1, S1 and S2, the considerable width of the characteristic XRD peaks indicates the nanocrystalline nature of the materials. Similar reports were found during the synthesis of UiO-66(Zr) using different approaches in water [1]. In general, achieving effective crystalline materials with narrow XRD reflections that resemble the reported patterns of conventional UiO-66(Zr) [1,55] and commercial UiO-66(Zr) is feasible using a mixed solvent approach. However, this process proves challenging when employing sustainable methods, which often result in semicrystalline Zr-BDC materials. The difficulty arises from the need for precise conditions to promote crystallinity while maintaining sustainability in the synthesis process. The encounter of metal dissolved in water M^{n+} with deprotonated carboxylate-based linker molecules $R(COO_2{}^-)_m$ provokes the instantaneous precipitation (rather than a crystallization event) of a solid metal carboxylate which has scarce chance to grow, as nucleation is completely favored over crystal growth. However, in the mixture of solvents strategy, the initially colorless solution starts to become cloudy after certain time, and then the cloudiness gradually becomes opaquer with time. In the latter case, nucleation and crystal growth phenomena can coexist, giving rise to nano-scaled UiO-66(Zr) crystals, which are more crystalline than the semicrystalline Zr-BDC entities.

The thermogravimetric profiles of the samples synthesized at 120 °C (the Nano-UiO-66(Zr) sample) and the commercial UiO-66(Zr) sample, along with the nanosized UiO-66(Zr) MOFs synthesized with zirconium oxychloride at room temperature, are shown in Figure 2. The profiles include those synthesized using two different strategies, with one synthesized in water with NaOH (the oxychloride sample) and the other synthesized with a water/DMF molar ratio of 1 (the oxychloride-1 sample). These profiles provide insight into the thermal stability and weight loss characteristics of the various UiO-66(Zr) materials under different synthesis conditions. Some other TGA curves of Zr-BDC samples are shown in Figure S3 and discussed in the Supporting Information. Table S2 collects some quantified data of different TGAs. The TGA curve of the Zr-BDC samples prepared from Zr acetate or Zr oxynitrate were quite similar to their counterparts prepared with Zr oxychloride. All the thermograms are in good agreement with previous reports made elsewhere [35] and show similar thermal stability to the commercial UiO-66(Zr) (Figure 2). Moreover, Table S3 presents the linker deficiencies of the most relevant UiO-66(Zr) samples from this study, calculated from the TGA profiles shown in Figure S3a,b, following the methodology described by Lillerud et al. [17]. The linker deficiency is notably high for the nanocrystalline sample of Nano-UiO-66(Zr), reaching a value of 1.6, corresponding to a molecular formula of $Zr_6O_{7.6}(BDC)_{4.4}$ when excluding OH groups. This sample exhibits a significant OH content, as indicated by the notable weight loss observed just above 200 °C (see Figures 2 and S3), which likely contributes to the high linker deficiency. In contrast, the UiO-66(Zr)-type materials prepared at room temperature also exhibit significant linker deficiencies, of approximately 1.3 (Table S3). This deficiency may be attributed to the semicrystalline nature of the MOF and the precipitation process that forms it, which typically results in the generation of defects within the resulting materials.

Figure 3 illustrates the N_2 sorption isotherms of the UiO-66(Zr)-type Zr-BDC samples synthesized from Zr oxychloride, Zr oxynitrate, and Zr acetate solution as Zr precursors, at room temperature and in water as the sole solvent, as well as the isotherm of a UiO-66(Zr)-type materials prepared through the mixture of solvents approach (water/DMF ratio of 3).

The specific BET surface area and other textural parameters are listed in Table S4. The porosity of the materials depends on the type of Zr precursor and the synthesis approach (Figure 3 and Table S4). The porosity of the as-synthesized materials is in a good agreement with previously reported works [35], but deviates to a certain extent from the report made by Cavka and co-workers [1] due to their semicrystalline nature. Moreover, the N_2 isotherms of all UiO-66-type materials display not only N_2 adsorption indicative of microporosity but also significant N_2 adsorption in the mesoporous region, characterized by notable hysteresis loops. This behavior suggests that the materials possess mesoporosity, which is further corroborated by the pore size distribution (PSD) of some selected samples (the same samples whose isotherms are presented in Figure 3), as illustrated in Figure S4. Unlike the commercial UiO-66(Zr) sample, the samples prepared at room temperature exhibit a certain level of mesoporosity (or at least some external surface area in the mesoporous range), though they do not reach the exceptional mesoporosity of the Nano-UiO-66(Zr) sample. The observed external surface area in the samples prepared at room temperature is presumably due to the agglomeration of semicrystalline nanodomains, forming larger micron-scale particles, as shown by the SEM and TEM images presented in Figures S5–S7.

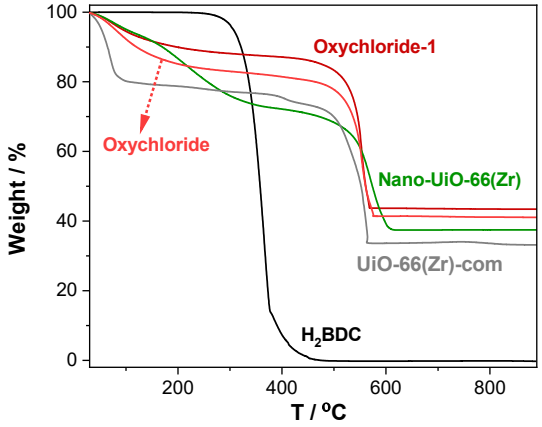


Figure 2. TGA curves of commercial UiO-66(Zr) (gray line), a nanosized UiO-66(Zr) (green), linker H_2BDC (black), the Zr-BDC MOFs obtained sustainably from Zr oxychloride (red), and the one synthesized at a water/DMF ratio of 1 (dark red), also prepared at room temperature.

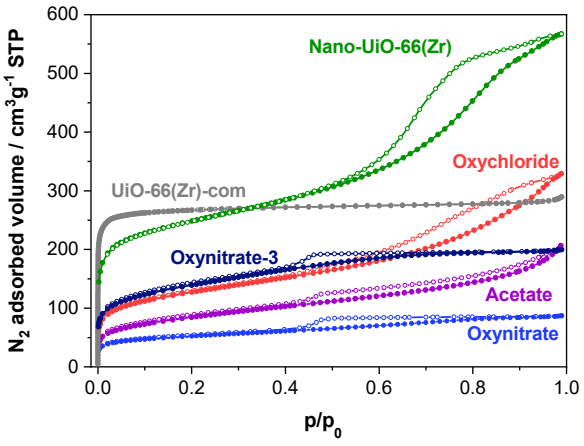


Figure 3. N_2 adsorption–desorption isotherms of UiO-type Zr-BDC MOFs synthesized in water with Zr oxychloride (red line), Zr oxynitrate (blue), and Zr acetate (purple), as well as the one prepared through the mixture of solvents approach (with water/DMF of 3) (dark blue). Isotherms of the nanocrystalline UiO-66(Zr) (red) and commercial UiO-66(Zr) (grey) are included for comparison purposes. Adsorption points are represented by full symbols whereas empty symbols correspond to desorption points.

The UV–Vis diffuse reflectance spectroscopy results (Figure S8 and Table S5), provide further evidence about the optical absorption, bandgap, and band alignments of samples obtained under both the sustainable and mixture of solvents approaches (see Section S6 of the Supplementary Materials). As expected, the bandgaps of the series of UiO-type Zr-BDC materials prepared at room temperature were very similar, with all of them in the range of 3.70–3.85 eV. Similarly, the FTIR-ATR spectra of the different RT-prepared Zr-BDC samples in this work are practically equal (Section S7 and Figure S9 of Supplementary Materials).

Figure 4 displays the photoluminescence (PL) spectra of the selected photocatalysts. The order of PL emission intensity among the UiO-type samples is as follows: oxychloride-1 > oxynitrate-1 > oxychloride > acetate-1 > oxynitrate. This trend suggests that the mixed solvents synthesis strategy, combined with the use of zirconium oxychloride as the Zr source, results in photocatalysts that exhibit the lowest recombination rates of photogenerated electron and hole pairs. This reduced recombination is advantageous for photocatalytic applications, as it enhances the efficiency of charge carrier utilization.

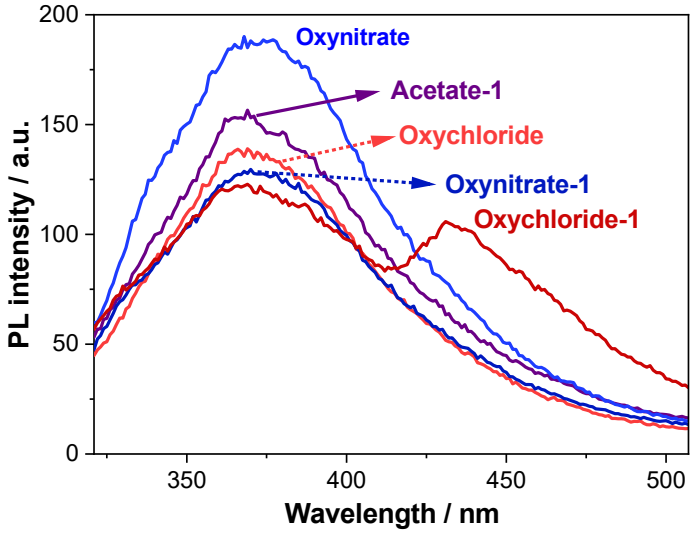


Figure 4. Photoluminescence (PL) spectra of UiO-type Zr-BDC MOFs prepared with different Zr precursors and with two different synthesis strategies.

2.2. Photocatalytic Degradation of Rhodamine B Dye

Rhodamine B (RhB) dye was chosen as a target organic pollutant to examine the photocatalytic potential of the RT-synthesized Zr-BDC samples with different Zr sources under mercury lamp irradiation. The effect of various factors, such as pH, catalyst load, contact time, and initial RhB concentration, on RhB dye photocatalytic activity were evaluated at room temperature (see Section S8 and Figure S10 of the Supplementary Materials).

Figure 5 shows the degradation of RhB by some of the Zr-BDC catalysts prepared at room temperature in this work. Thus, the samples prepared in water using NaOH as deprotonating agent with Zr oxychloride, oxynitrate, and acetate as Zr precursors were able to remove 66%, 41%, and 53% of RhB, respectively, after 120 min of the reaction (Figure 5a). On the other hand, the counterparts prepared through the solvent mixture strategy using either Zr oxychloride or Zr oxynitrate as Zr sources became even more photoactive, with 75% and 69% of RhB degradation under pseudo-first-order model (Table S6), respectively (Figure 5b), along with rate constant values of 0.011 and 0.009 min^{-1}, respectively. Meanwhile, the acetate-1 and chloride-1 samples evidenced lower photocatalytic efficiencies (45 and 44%, respectively) (Figure 5b). This decomposition efficiency is comparable with earlier reports, where UiO-66(Zr) materials were used for the removal of other dyes [56–58], or where other MOFs were employed in the photodegradation of the same dye, namely

RhB (Table S7). It is remarkable that the Zr-BDC materials prepared at room temperature by both synthesis strategies lead to a different kinetics of RhB degradation according to the pseudo-first order kinetic model (Figure S11a,b). Thus, the materials prepared by linker deprotonation in water are able to remove a greater amount of the dye in shorter times, probably because of their mesoporosity/external surfaces, as detected by the N_2 isotherms (Figure 3 and Table S4), making easier for the dye molecules to access the active centers. Meanwhile, the samples prepared using the solvent mixture strategy, particularly those synthesized with Zr oxychloride or oxynitrate—the most active samples—exhibit a steeper slope over a longer period in the degradation kinetics. Moreover, the observed degradation during the light-off phase (Figure 5a,b) is attributed to adsorption and not to photocatalytic activity. When the light is turned off, the RhB's adsorbed molecules on the photocatalyst surface suffer gradual photodegradation. Additionally, the porous structure of the material may facilitate this adsorption, further enhancing the removal of RhB dye from the solution.

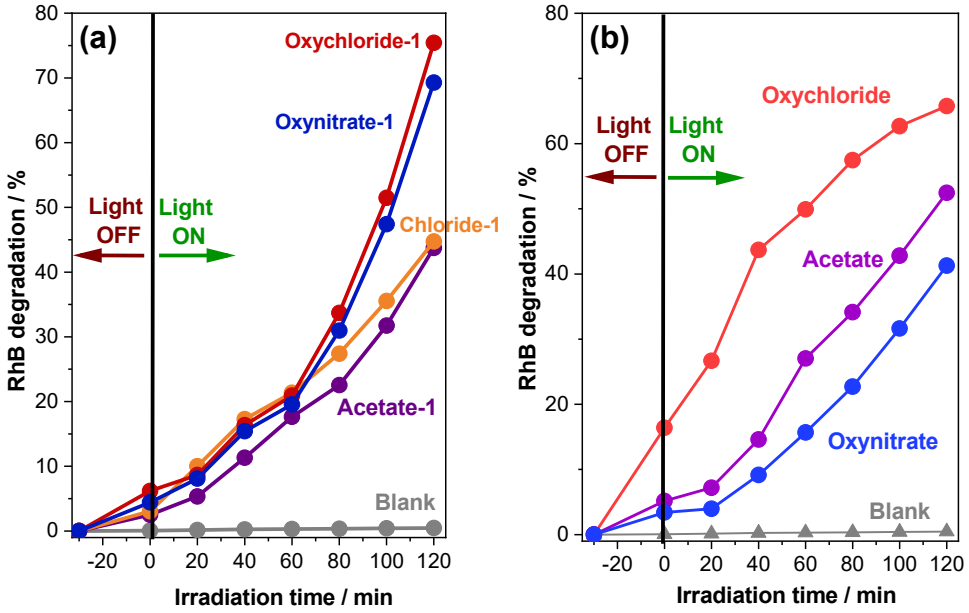


Figure 5. Kinetics of RhB degradation by Zr-BDC prepared at room temperature with different Zr precursors in water/NaOH (**a**) or in water/DMF (**b**). The reaction conditions were as follows: mercury lamp as a light source (85 W), the distance between the top of the reactor and the lamp was 10 cm, catalyst loading of 60 mg L^{-1}, RhB concentration of 10 mg L^{-1}, and 120 min of reaction time.

The reusability of the photocatalyst is a primary concern for industrial applications and related practical uses. Therefore, the reusability of the most active photocatalyst, oxychloride-1, was evaluated through five repeated cycles under identical reaction conditions (Figure 6a). The photocatalytic discoloration efficiencies for the first five cycles were 75.4%, 71.2%, 68.5%, 65.6%, and 63.9%, respectively, strongly suggesting the feasibility of recycling these materials. The slight weight loss of approximately 2–3 mg in each cycle could explain the decrease in discoloration efficiency from 75.4% to 63.9%, as this results from the use a reduced amount of catalyst to degrade the same volume and concentration of aqueous RhB solution. Additionally, the same sample was tested under dark conditions, where an RhB adsorption of 36.6% was observed after 120 min, compared to 75.4% under light irradiation (Figure 6b). This indicates that mercury lamp radiation is crucial for achieving such high dye degradation. While adsorption is vital for facilitating the photocatalytic process—since dye molecules must first be adsorbed onto the material's surface before photodegradation—the substantial improvement in degradation efficiency under light confirms the significant role of the mercury lamp in driving the photocatalytic reaction. In contrast, a blank experiment (with no catalyst) showed almost negligible degradation. In

summary, this as-synthesized Zr-BDC photocatalyst is easily recyclable and maintains high discoloration efficiency for RhB.

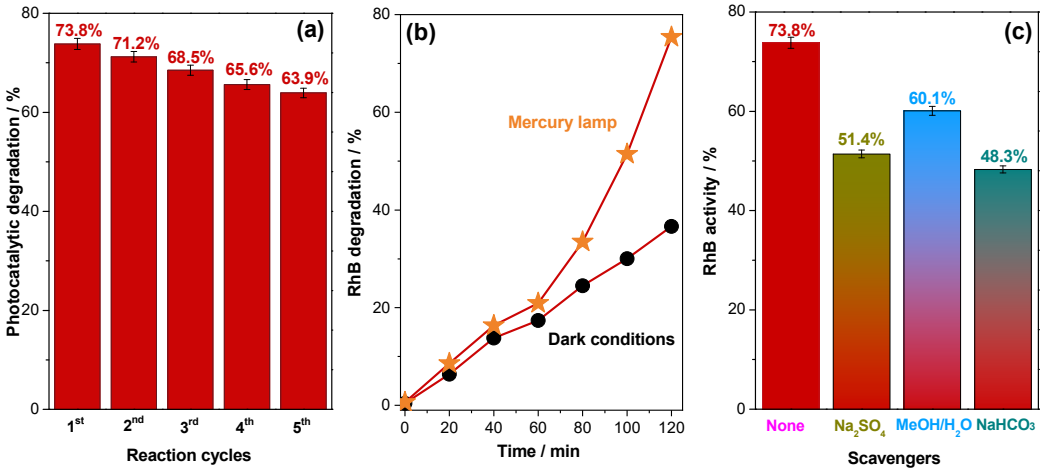


Figure 6. (**a**) RhB degradation given by the oxychloride-1 sample in five consecutive cycles. (**b**) Kinetics of % RhB degradation given by oxychloride-1 under mercury lamp irradiation and under dark conditions. (**c**) Effect of the trapping agents (scavengers) on the photocatalytic reaction of RhB by the oxychloride-1 sample under mercury lamp irradiation. Reaction conditions: catalyst loading of 60 mg of UiO-66(Zr) (1:1), RhB concentration of 10 mg L^{-1}, 120 min of reaction time, pH = 10, and a mercury lamp as a light source (85 W); the distance between the top of the reactor and the lamp was 10 cm.

To understand the contribution of the possible photoactive species, sodium sulphate (Na_2SO_4), sodium hydrogen carbonate ($NaHCO_3$), and methanol/water ($MeOH/H_2O$) were used as the trapping agents/scavengers for superoxide radicals ($^{\bullet}O_2^-$), photogenerated holes (h^+), and hydroxyl radicals ($^{\bullet}OH$) in RhB solution (Figure 6c) [35,59,60]. These different quenching experiments were also carried out using the oxychloride-1 sample as a photocatalyst under the same reaction conditions. The photocatalytic discoloration of RhB dye decreased upon the addition of methanol/water (60.1%), suggesting that hydroxyl radicals ($^{\bullet}OH$) have certain influence on the RhB discoloration process. Meanwhile, after adding sodium sulphate and sodium hydrogen carbonate scavengers into the solution, the photocatalytic activity was significantly affected (51.4 and 48.3%, respectively). This indicates that the superoxide radicals and photogenerated holes (h^+) are the dominant active intermediates. In addition, hydroxyl radicals were also involved in the discoloration process of RhB to water and carbon dioxide compared with superoxide radicals ($^{\bullet}O_2^-$), which were not [61].

In order to understand the photogenerated charge separation, it is imperative to estimate the flat band potentials and band gap energies of the photocatalysts involved [35]. The photocatalytic process was started by the absorption of photon energy (from the mercury lamp) equal to or greater than the band gap of the oxychloride-1 sample ($h\nu \geq 3.83$ eV), while the photogenerated electrons came from the RhB dye material. To elucidate the photocatalytic activity, the valance band (VB) and conduction band (CB) edge position of the oxychloride-1 photocatalyst were estimated using the $E_{VB} = X - E_o + 0.5Eg$ and $E_{CB} = E_{VB} - Eg$ equations, where Eg is band gap energy, E_{VB} is VB energy, E_{CB} is CB energy, and X is the absolute electronegativity of semiconductor. The X value of oxychloride-1 is 6.2 eV. E_o is the energy of free electrons on the hydrogen scale, i.e., 4.5 eV [35]. The band gap value of oxychloride is 3.83 eV (Table S5), whereas the values of the CB and VB for oxychloride-1 are −0.22 eV and +3.62 eV (vs. NHE), respectively. However, the electrons in the CB of oxychloride-1 cannot reduce dissolved oxygen to superoxide radicals fully

by itself due to the CB potential (−0.22 eV vs. NHE) being slightly more positive than that of the potential of $O_2/{}^{\bullet}O_2^-$ (−0.33 eV or −0.33 V vs. NHE) [62–64]. Interestingly, the electron on the LUMO of RhB can transfer to the LUMO of the BDC linker in Zr-BDC oxychloride-1 due to the largest charge transfer ability of RhB under irradiation [53,54], and the electron directly moved to the Zr-oxo cluster via ligand to metal charge transfer (LMCT). This simultaneously creates the electronic interaction between oxychloride and RhB dye in solution [65], causing the reduction of Zr^{4+} to Zr^{3+}. Noticeably, LMCT is the principal mechanism to prevent electron–hole recombination, in which the excited electrons are transferred from the organic linkers to the metal nodes [66]. These injected and/or transferred electrons react with O_2 molecules on the surface of oxychloride-1 to form superoxide anion radicals via reduction to degrade RhB to water and carbon dioxide products, due to the high intervalence potential of Zr^{3+}/Zr^{4+}, redox behavior, or the negative E_{LMCT} of the oxychloride-1 MOF. In addition, thanks to the presence of RhB, the photogenerated charge separations are facilitated, resulting in efficient photocatalytic decolorization of RhB. The photogenerated holes in the VB of oxychloride-1 is sufficient to react with the adsorbed water molecules to produce hydroxyl radicals due it having a greater positive potential value than the standard redox potential (${}^{\bullet}OH/H_2O$ = +2.8 eV or +2.8 V vs. NHE) and ${}^{\bullet}OH/OH^-$ (+2.38 eV or +2.38 V vs. NHE) [63,64,67]. For RhB dye, the CB and VB energy values are −1.42 eV and +0.96 eV (vs. NHE), respectively [54].

Based on this information, the plausible methods of electron transfer were proposed in Figure 7. Since oxychloride-1 comprise higher valance edge potential (+3.62 eV vs. NHE) associated with the redox potentials of ${}^{\bullet}OH/H_2O$ of +2.8 eV vs. NHE and ${}^{\bullet}OH/OH^-$ of +2.38 eV vs. NHE, it easily oxidizes H_2O and OH^- to hydroxyl radicals (${}^{\bullet}OH$), indicating that the photoinduced holes on the VB of oxychloride-1 facilitate the photocatalytic reaction. The photogenerated holes and hydroxyl radicals of oxychloride-1 as well as the transferred electrons on surface of CB of photocatalysts are crucial reactive intermediates for oxidizing and reducing RhB dye directly under mercury lamp irradiation [68], which is in good agreement with the results of quenching experiments.

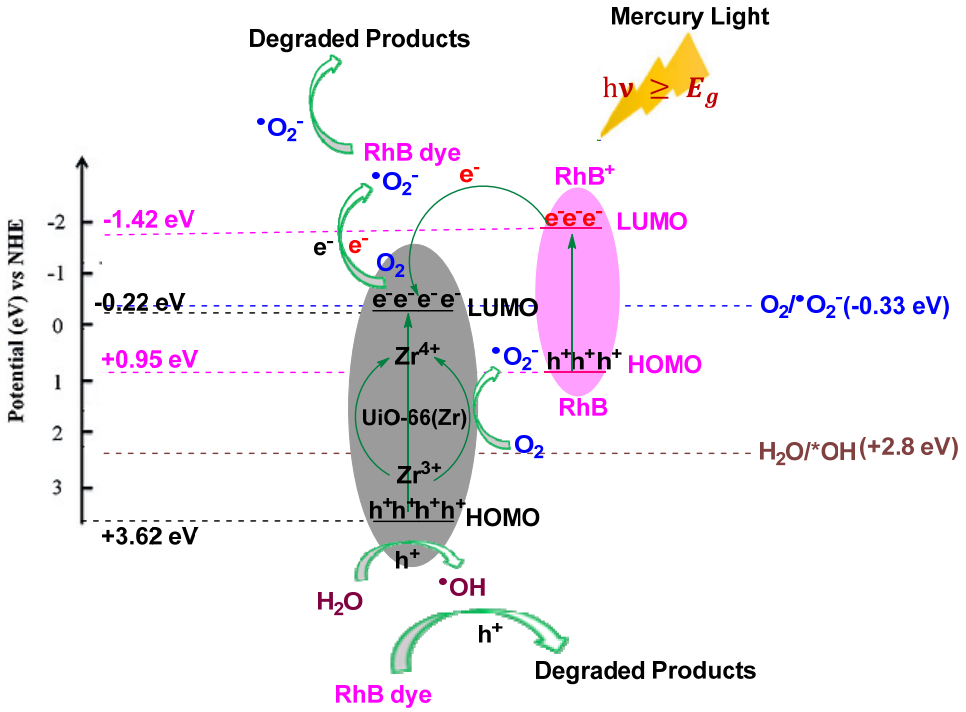


Figure 7. Proposed mechanism for RhB degradation by the reactive species of the oxychloride-1 photocatalyst under mercury lamp irradiation.

3. Materials and Methods

3.1. Reagents and Chemicals

Zirconium oxychloride octahydrate ($ZrOCl_2 \cdot 8H_2O$, Sigma Aldrich, >99.9%, St. Louis, MO, USA), zirconium oxynitrate hydrate ($ZrO(NO_3)_2 \cdot xH_2O$, Sigma Aldrich, >99.9%, St. Louis, MO, USA), zirconium chloride ($ZrCl_4$, Alfa Aesar, 99.5+%, St. Quentin Fallavier, France), zirconium (IV) acetate solution in dilute acetic acid ($C_8H_{12}O_8Zr$, 15.0–17.0% gravimetric of Zr, Sigma Aldrich, >99.9%, St. Louis, MO, USA), terephthalic acid ($C_8H_6O_4$, Acrōs organics, 99.7%, Geel, Belgium), sodium hydroxide (1.0 M NaOH), acetone (C_3H_6O, Scharlab, Scharlau multi-solvent, HPLC grade, Barcelona, Spain), *N*,*N*-dimethylformamide (DMF, Scharlau multi-solvent, HPLC grade, Barcelona, Spain), methanol (CH_3OH, Panreac AppliChem, 99.5%, Barcelona, Spain), ethanol (C_2H_5OH, Scharlau, gradient HPLC grade, Barcelona, Spain), and rhodamine B dye (RhB, $C_{28}H_{31}ClN_2O_3$, Sigma Aldrich, ≥99.9%, Bangalore, India) were purchased and used without further purifications. A commercial UiO-66(Zr), purchased from Strem Chemicals, was used for comparison purposes.

3.2. Synthesis of MOFs

The sustainable synthesis of semicrystalline UiO-type Zr-BDC MOF using an equimolar ratio of zirconium oxynitrate and H_2BDC linker was carried out in water in the presence of NaOH as a deprotonating agent at room temperature. Typically, 1.399 g of $ZrO(NO_3)_2 \cdot xH_2O$ (6.05 mmol) was dissolved in 28 mL of distilled water (solution 1) and 1.01 g of H_2BDC (6.05 mmol) was dissolved in 22 mL of distilled water in separate Pyrex glasses. Then 13 mL of NaOH solution (1.0 M) was slowly added to the linker suspension, then stirred for 30 min until a clear solution (solution 2) was obtained. Solution 1 was transferred dropwise into solution 2, and then the white resultant suspension was stirred for 24 h at room temperature; the white solid was called Oxynitrate. A similar product was obtained by using zirconium oxychloride (sample Oxychloride) [35], and zirconium (IV) acetate solution (sample Acetate) precursors under the same experimental conditions, while zirconium chloride is scarcely soluble in water and it was not considered in this approach. The formed solid precipitate was centrifuged at 2500 rpm for 15 min and washed with distilled water (three times, ×3) and subsequently with ethanol (twice, ×2). Some other samples were prepared over a period shorter than 24 h to study the effect of the kinetics.

Alternatively, nanosized UiO-66(Zr) was successfully synthesized at room temperature using different water/DMF molar ratios of solvents, keeping constant the solvent molar ratios across the various zirconium precursors, all without deprotonating agents, modulators, or other additives. This strategy maintained the same metal/linker molar ratio (Table S1). For the synthesis, 0.322 g (1 mmol) of zirconium oxychloride octahydrate was dissolved in either 2.7 mL (150 mmol) (solution 1) or in 1.8 mL (100 mmol) (solution 2) or in 0.9 mL (50 mmol) (solution 3) of distilled water or in 7.30 g (100 mmol) DMF solvent (solution 4) under stirring for 30 min. Simultaneously, 0.166 g (1 mmol) of terephthalic acid (H_2BDC) was dissolved in either 3.65 g (50 mmol) (solution 5) or in 7.30 g (100 mmol) (solution 6) or 10.96 g (150 mmol) (solution 7) or 7.30 g (100 mmol) (solution 8) of DMF. Thus, solution 1 was transferred into solution 5. In the same regard, solution 2 was transferred into solution 6, solution 3 into solution 7 and solution 4 into solution 8 dropwise to obtain the sought-after product, namely UiO-66(Zr)-DMF. Unlike the first strategy, the formation of precipitate was not instantaneous right after mixing both solutions; the mixture required a few minutes to become cloudy and a longer time (from 24 h to 96 h, with increasing DMF/water molar ratio) to complete the precipitation. The precipitate was collected via centrifugation at 3750 rpm for 15 min, and the solid was washed with water (three times, ×3), ethanol (twice, ×2) and soaked in acetone several times overnight. Finally, the thus-obtained solid was dried at 80 °C overnight. Similar experiments were

conducted using other Zr precursors, such as Zr-oxynitrate, Zr-chloride, and Zr-acetate. The products were denoted as Precursor-r, where r stands for the water/DMF molar ratio (Table S1), which was 3, 1, or 0.33. For comparison, a nanocrystalline UiO-66(Zr) was prepared using zirconium oxychloride octahydrate precursor under solvothermal methods and labeled as Nano-UiO-66(Zr) [6]. In addition, commercial UiO-66(Zr) was used as a reference material (UiO-66(Zr)-com).

3.3. Materials Characterization

The synthesized materials were characterized using various advanced techniques. Powder X-ray diffraction (PXRD) using a Philips X'PERT diffractometer (PANalytical, Almelo, The Netherlands) equipped with an X'Celerator detector and Cu Kα radiation (λ = 1.5418 Å) was employed to identify the crystalline structure and phase purity. N_2 sorption properties were measured at −196 °C using a Micromeritics instrument, namely an ASAP 2420 device (Micromeritics Instrument Corporation, Norcross, GA, USA). Typically, before measurements of any isotherms, approximately 100 mg of each sample was prepared and outgassed at 150 °C for 16 h under high vacuum. Thus, the surface area of the materials was estimated using the Brunauer–Emmet–Teller (BET) method. Micropore and external surface area was determined by the t-plot method. The total pore volume were measured at relative pressure p/p_0 of 0.98. Thermogravimetric analysis (TGA) was performed using a Perkin-Elmer TGA7 instrument (PerkinElmer, Waltham, MA, USA), in the temperature range of 30 °C to 900 °C under air flow and at a constant heating rate of 20 °C min^{-1}. Scanning electron microscopy and energy dispersive X-ray spectroscopy (SEM-EDS) were carried out using a Hitachi Tabletop Microscope TM1000 (Hitachi High-Technologies Corporation, Tokyo, Japan) with a tungsten filament electron gun to detect the morphology and elemental composition of materials. FTIR-ATR (PerkinElmer, MA, USA) spectrometry was employed to identify the functional groups of as-synthesized samples. UV–Vis diffuse reflectance spectroscopy (DRS) measurements were made using a Varian Cary 5000 double-beam UV–Vis near-IR spectrophotometer (Agilent Technologies, Santa Clara, CA, USA). The collected spectra of the photocatalysts were converted to their Kubelka–Munk function, i.e., F(R) versus wavelength. Photoluminescence (PL) spectra were determined using a SHIMADZU, RF-5301PC (LABQUIP, Manchester, UK) spectrofluorophotometer.

3.4. Photocatalytic Experiments

The photocatalytic degradation of RhB was performed using the as-synthesized UiO-type Zr-BDC MOFs prepared from different Zr precursors through both a sustainable approach and by using a mixture of solvents (water and DMF) under the irradiation of a mercury vapor lamp. Typically, 60 mg of the as-synthesized photocatalyst was dispersed into 100 mL of an RhB (10 mg L^{-1}) aqueous solution in a 250 mL beaker at room temperature with continuous stirring under dark condition for 30 min to achieve an adsorption–desorption equilibrium before starting the irradiation. During the photocatalytic process, the suspension in the reactor was irradiated with 85-watt mercury lamp as a light source with a continuous oxygen supply under stirring. Then, 4 mL of the solution was removed at the specified time and centrifuged, and its absorbance was measured (A_0 in the dark after 0 min, and At after 20 min intervals). For comparison, the dark and blank (with no catalyst) experiments were also carried out under similar protocol.

To evaluate the reusability of the selected photocatalyst, five consecutive cycles were conducted under optimized reaction conditions. The solid catalyst was separated by centrifugation after each cycle and washed with water (three times, ×3) and ethanol (twice, ×2) to remove the retained RhB dye and then dried at 60 °C overnight. In addition, the contributions of active species in the photocatalytic reaction were evaluated by following

the previous reports [35,59], using various scavengers, such as 10 mL of 0.1 M each of sodium sulphate, sodium hydrogen carbonate, and methanol/water separately, which were introduced into the RhB solution before the addition of the photocatalyst to trap superoxide radicals ($^{\bullet}O_2^-$), photogenerated holes (h^+), and hydroxyl radicals ($^{\bullet}OH$), respectively.

4. Conclusions

This work provides new and valuable insights into the sustainable synthesis of UiO-type semi-crystalline Zr-BDC metal–organic frameworks (MOFs) using equimolar ratios of various zirconium precursors and terephthalic linker (H_2BDC) through different systematic approaches at room temperature. Our synthesis methods are more competitive, being notably easier, more economical, rapid, and sustainable compared to conventional synthesis methodologies. The physicochemical properties of the as-synthesized materials revealed that they are nanosized materials with excellent thermal stability and relatively high specific surface areas, paving the way towards a pilot-scale fabrication of these materials. Moreover, the UiO-66(Zr) sample prepared using Zr oxychloride as the Zr precursor in a mixture of solvents (water/DMF at a molar ratio of 1) showed the best photodegradation of RhB under mercury light irradiation. The trapping experiment confirms that both superoxide radicals and photogenerated holes (h^+) are the dominant active species. The selected photocatalyst is easily recyclable and shows high discoloration efficiency for RhB even after five repeated cycles. This capability allows the photocatalyst to be reused effectively across different cycles, making it a promising candidate for practical applications in dye degradation and environmental remediation.

Supplementary Materials: The following supporting information can be downloaded at: https://www.mdpi.com/article/10.3390/inorganics13050131/s1, Figure S1: (a) Before background-removed normalized PXRD patterns of sustainable synthesized UiO type Zr-BDC prepared from Zr-oxychloride, Zr-oxynitrate, and Zr-acetate. (b) PXRD patterns of the Zr-BDC prepared from Zr-oxynitrate after 30 min, 2 h, 24 h and 48 h. The simulated XRD pattern of UiO-66(Zr) and the experimental XRD patterns of UiO-commercial and nanocrystalline UiO-66(Zr) prepared at high temperature (sample Nano-UiO-66(Zr)) is shown for comparison purposes; Figure S2: PXRD patterns of Zr-BDC prepared with (a) Zr-oxychloride and (b) Zr-oxynitrate with different water/DMF molar ratio of solvents. PXRD patterns of a commercial UiO-66(Zr) and a nanocrystalline UiO-66(Zr) prepared at room temperature (sample Nano-UiO-66(Zr)), as well as the simulated PXRD pattern of a UiO-66(Zr), are shown for comparison purposes; Figure S3: TGA curves of Zr-BDC samples prepared with Zr-oxychloride (red), Zr oxynitrate (blue) and Zr acetate (purple). TGA profiles of a commercial UiO-66(Zr) (gray), solvothermally-prepared Nano-UiO-66(Zr) (green) and protonated H_2BDC linker (black) are shown for comparative purposes; and (b) The normalized TGA profiles of conventional UiO-66(Zr) (the commercial one, gray), the nanocrystalline UiO-66(Zr) (green) and the semicrystalline UiO-66(Zr)-type material (sample Oxychloride) (red) for linker deficiency calculation; Figure S4: Pore size distribution curves from the adsorption branches of the isotherms of Zr-BDC samples prepared at room temperature shown in Figure 4: in water with Zr-oxychloride (red), Zr oxynitrate (blue) and Zr acetate (purple), and in a mixture of solvents (water/DMF molar ratio of 3). PSD profiles of a commercial UiO-66(Zr) (gray), solvothermally-prepared Nano-UiO-66(Zr) (green) and protonated H2BDC linker (black) are shown for comparative purposes; Figure S5: SEM micrographs of the sample Oxychoride with magnifications of 16,000 (a) and 30,000 (b) magnifications. Micrographs registered in a microscope Philips XL 30 SEM; Figure S6: SEM micrographs of the sample Oxychloride-3 registered with different magnifications. Micrographs registered in a Tabletop TM-1000 Microscope (Hitachi); Figure S7: TEM micrographs at different magnifications of the sample Oxychoride. Micrographs registered in a JEOL 2000FX microscope operated with an accelerating voltage of 200 kV; Figure S8: (a) DR-UV-vis spectra and (b) Tauc plots of UiO type Zr-BDC prepared at room temperature starting from Zr oxychloride, Zr oxynitrate and Zr acetate by two different methodologies: in NaOH/water and in mixture of solvents with water/DMF molar ratio of 1. In Figure S6b,

dotted green lines indicate the different projections of the UV-vis signal to estimate the band gap of each sample by cutting with the X-axis; Figure S9: FTIR-ATR spectra of the Zr-BDC samples prepared at room temperature with Zr oxychloride under different synthesis strategies/conditions (a) and with different Zr precursors under given conditions (mixture of solvents with a water/DMF ratio of 1). The corresponding FTIR-ATR spectra of the commercial UiO-66(Zr) (grey line) and Nano-UiO-66(Zr) (green) are shown in both Figures for comparison purposes; Figure S10: Kinetics of RhB degradation as a function of (a) pH and (b) catalyst loading. Reaction conditions: mercury lamp as a light source (85 W), the distance between the top of the reactor and the lamp was 10 cm, RhB concentration of 10 mg L^{-1}, and 120 min of reaction time under mercury light irradiation; Figure S11: Plots of $\ln(C_0/C_t)$ versus reaction time for RhB degradation using various photocatalysts under mercury lamp irradiation. A blank experiment (without catalyst) is included (dark grey) for comparison, illustrating the reaction kinetics; Table S1: Different water/DMF molar ratio in the synthesis of Zr-BDC at room temperature using different Zr precursors; Table S2: Thermogravimetric analysis profiles of as-synthesized UiO type Zr-BDC and UiO-66(Zr) samples at room temperature using different Zr precursors in different approaches; Table S3: Quantitative data were obtained from the TGA traces using the methodology described in previous work; Table S4: Textural properties of the different Zr-BDC samples; Table S5: Band gap of the synthesized MOFs photocatalysts; Table S6: The average degradation efficiency of RhB after 120 min under mercury lamp irradiation; Table S7: Comparison of our Zr-BDC photocatalysts versus other reported ones in the degradation of RhB; References [69–81] are cited in the Supplementary Materials.

Author Contributions: Conceptualization, J.M.Y., A.M.T. and M.S.-S.; methodology, J.M.Y. and M.S.-S.; software, M.S.-S.; validation, J.M.Y.; formal analysis, J.M.Y.; investigation, J.M.Y. and M.S.-S.; resources, J.M.Y., A.M.T. and M.S.-S.; data curation, J.M.Y., A.M.T. and M.S.-S.; writing—original draft preparation, J.M.Y.; writing—review and editing, J.M.Y., A.M.T. and M.S.-S.; visualization, J.M.Y., A.M.T. and M.S.-S.; supervision, A.M.T. and M.S.-S.; project administration, J.M.Y., A.M.T. and M.S.-S.; funding acquisition, J.M.Y., A.M.T. and M.S.-S. All authors have read and agreed to the published version of the manuscript.

Funding: The authors acknowledge the Spanish Research Council CSIC for funding through the projects COOPB22002 and COOPB24072. This research work was also financially supported by Haramaya University (HURG-2020-03-02-75, Ethiopia) and Debre Berhan University. MSS acknowledges the projects TED2021-131143B-I00 and PID2022-136321OB-C21, funded by MCIN/AEI/10.13039/501100011033 and the European Union "NextGenerationEU"/PRTR and MCIN/AEI/10.13039/501100011033 and FEDER, respectively.

Data Availability Statement: Data are contained within the article.

Acknowledgments: The authors acknowledge the people from 'Unidad de Apoyo' for their assistance in registering the XRD and N_2 isotherms analyses.

Conflicts of Interest: The authors declare no conflicts of interest.

References

1. Cavka, J.H.; Jakobsen, S.; Olsbye, U.; Guillou, N.; Lamberti, C.; Bordiga, S.; Lillerud, K.P. A new zirconium inorganic building brick forming metal organic frameworks with exceptional stability. *J. Am. Chem. Soc.* **2008**, *130*, 13850–13851. [CrossRef]
2. Hendon, C.H.; Rieth, A.J.; Korzyński, M.D.; Dincă, M. Grand challenges and future opportunities for metal–organic frameworks. *ACS Cent. Sci.* **2017**, *3*, 554–563. [CrossRef] [PubMed]
3. Yuan, S.; Feng, L.; Wang, K.; Pang, J.; Bosch, M.; Lollar, C.; Sun, Y.; Qin, J.; Yang, X.; Zhang, P. Stable metal–organic frameworks: Design, synthesis, and applications. *Adv. Mater.* **2018**, *30*, 1704303. [CrossRef] [PubMed]
4. He, T.; Kong, X.-J.; Li, J.-R. Chemically stable metal–organic frameworks: Rational construction and application expansion. *Acc. Chem. Res.* **2021**, *54*, 3083–3094. [CrossRef] [PubMed]
5. Zhang, Y.; Liu, H.; Gao, F.; Tan, X.; Cai, Y.; Hu, B.; Huang, Q.; Fang, M.; Wang, X. Application of MOFs and COFs for photocatalysis in CO_2 reduction, H_2 generation, and environmental treatment. *EnergyChem* **2022**, *4*, 100078. [CrossRef]
6. Wang, Q.; Yang, G.; Fu, Y.; Li, N.; Hao, D.; Ma, S. Nanospace Engineering of Metal-Organic Frameworks for Heterogeneous Catalysis. *ChemNanoMat* **2022**, *8*, e202100396. [CrossRef]

7. Yassin, J.M.; Taddesse, A.M.; Tsegaye, A.A.; Sánchez-Sánchez, M. CdS/g-C_3N_4/Sm-BDC MOF nanocomposite modified glassy carbon electrodes as a highly sensitive electrochemical sensor for malathion. *Appl. Surf. Sci.* **2024**, *648*, 158973. [CrossRef]
8. Belaye, M.; Taddesse, A.M.; Teju, E.; Sanchez-Sanchez, M.; Yassin, J.M. Preparation and adsorption behavior of Ce (III)-MOF for phosphate and fluoride ion removal from aqueous solutions. *ACS Omega* **2023**, *8*, 23860–23869. [CrossRef]
9. D'Amato, R.; Donnadio, A.; Carta, M.; Sangregorio, C.; Tiana, D.; Vivani, R.; Taddei, M.; Costantino, F. Water-Based Synthesis and Enhanced CO_2 Capture Performance of Perfluorinated Cerium-Based Metal–Organic Frameworks with UiO-66 and MIL-140 Topology. *ACS Sustain. Chem. Eng.* **2018**, *7*, 394–402. [CrossRef]
10. Sánchez-Sánchez, M.; Getachew, N.; Díaz, K.; Díaz-García, M.; Chebude, Y.; Díaz, I. Synthesis of metal–organic frameworks in water at room temperature: Salts as linker sources. *Green Chem.* **2015**, *17*, 1500–1509. [CrossRef]
11. Li, D.; Xu, H.-Q.; Jiao, L.; Jiang, H.-L. Metal-organic frameworks for catalysis: State of the art, challenges, and opportunities. *EnergyChem* **2019**, *1*, 100005. [CrossRef]
12. DeStefano, M.R.; Islamoglu, T.; Garibay, S.J.; Hupp, J.T.; Farha, O.K. Room-temperature synthesis of UiO-66 and thermal modulation of densities of defect sites. *Chem. Mater.* **2017**, *29*, 1357–1361. [CrossRef]
13. Yassin, J.M.; Taddesse, A.M.; Sánchez-Sánchez, M. Room temperature synthesis of high-quality Ce (IV)-based MOFs in water. *Microporous Mesoporous Mater.* **2021**, *324*, 111303. [CrossRef]
14. Avci-Camur, C.; Perez-Carvajal, J.; Imaz, I.; Maspoch, D. Metal acetylacetonates as a source of metals for aqueous synthesis of metal–organic frameworks. *ACS Sustain. Chem. Eng.* **2018**, *6*, 14554–14560. [CrossRef]
15. Wu, H.; Chua, Y.S.; Krungleviciute, V.; Tyagi, M.; Chen, P.; Yildirim, T.; Zhou, W. Unusual and highly tunable missing-linker defects in zirconium metal–organic framework UiO-66 and their important effects on gas adsorption. *J. Am. Chem. Soc.* **2013**, *135*, 10525–10532. [CrossRef]
16. Czaja, A.U.; Trukhan, N.; Müller, U. Industrial applications of metal–organic frameworks. *Chem. Soc. Rev.* **2009**, *38*, 1284–1293. [CrossRef]
17. Shearer, G.C.; Chavan, S.; Bordiga, S.; Svelle, S.; Olsbye, U.; Lillerud, K.P. Defect engineering: Tuning the porosity and composition of the metal–organic framework UiO-66 via modulated synthesis. *Chem. Mater.* **2016**, *28*, 3749–3761. [CrossRef]
18. Morris, W.; Wang, S.; Cho, D.; Auyeung, E.; Li, P.; Farha, O.K.; Mirkin, C.A. Role of modulators in controlling the colloidal stability and polydispersity of the UiO-66 metal–organic framework. *ACS Appl. Mater. Interfaces* **2017**, *9*, 33413–33418. [CrossRef]
19. Guillerm, V.; Gross, S.; Serre, C.; Devic, T.; Bauer, M.; Férey, G. A zirconium methacrylate oxocluster as precursor for the low-temperature synthesis of porous zirconium (IV) dicarboxylates. *Chem. Commun.* **2010**, *46*, 767–769. [CrossRef]
20. Dai, S.; Nouar, F.; Zhang, S.; Tissot, A.; Serre, C. One-Step Room-Temperature Synthesis of Metal (IV) Carboxylate Metal—Organic Frameworks. *Angew. Chem. Int. Ed.* **2021**, *133*, 4328–4334. [CrossRef]
21. Jerozal, R.T.; Pitt, T.A.; MacMillan, S.N.; Milner, P.J. High-Concentration Self-Assembly of Zirconium-and Hafnium-Based Metal–Organic Materials. *J. Am. Chem. Soc.* **2023**, *145*, 13273–13283. [CrossRef] [PubMed]
22. Fu, J.; Wu, Y.n. A showcase of green chemistry: Sustainable synthetic approach of zirconium-based MOF materials. *Chem. Eur. J.* **2021**, *27*, 9967–9987. [CrossRef] [PubMed]
23. Hu, Z.; Peng, Y.; Kang, Z.; Qian, Y.; Zhao, D. A modulated hydrothermal (MHT) approach for the facile synthesis of UiO-66-type MOFs. *Inorg. Chem.* **2015**, *54*, 4862–4868. [CrossRef] [PubMed]
24. Hu, Z.; Castano, I.; Wang, S.; Wang, Y.; Peng, Y.; Qian, Y.; Chi, C.; Wang, X.; Zhao, D. Modulator effects on the water-based synthesis of Zr/Hf metal–organic frameworks: Quantitative relationship studies between modulator, synthetic condition, and performance. *Cryst. Growth Des.* **2016**, *16*, 2295–2301. [CrossRef]
25. Kim, Y.; Lam, I.T.Y.; Choi, S.-J.; Lu, D. Functionalized Metal–Organic Frameworks for Heavy Metal Ion Removal from Water. *Nanoscale* **2023**, *15*, 10189–10205. [CrossRef]
26. Chen, Z.; Wang, X.; Noh, H.; Ayoub, G.; Peterson, G.W.; Buru, C.T.; Islamoglu, T.; Farha, O.K. Scalable, room temperature, and water-based synthesis of functionalized zirconium-based metal–organic frameworks for toxic chemical removal. *CrystEngComm* **2019**, *21*, 2409–2415. [CrossRef]
27. Guo, D.; Li, H.; Wang, J.; Xu, Z. Facile synthesis of NH_2-UiO-66 modified low-cost loofah sponge for the adsorption of fluoride from water. *J. Alloys Compd.* **2022**, *929*, 167270. [CrossRef]
28. Kalaj, M.; Prosser, K.E.; Cohen, S.M. Room temperature aqueous synthesis of UiO-66 derivatives via postsynthetic exchange. *Dalton Trans.* **2020**, *49*, 8841–8845. [CrossRef]
29. Li, K.; Yang, J.; Gu, J. Salting-in species induced self-assembly of stable MOFs. *Chem. Sci.* **2019**, *10*, 5743–5748. [CrossRef]
30. Dai, S.; Tissot, A.; Serre, C. Metal-organic frameworks: From ambient green synthesis to applications. *Bull. Chem. Soc. Jpn.* **2021**, *94*, 2623–2636. [CrossRef]
31. Zou, C.; Vagin, S.; Kronast, A.; Rieger, B. Template mediated and solvent-free route to a variety of UiO-66 metal–organic frameworks. *RSC Adv.* **2016**, *6*, 102968–102971. [CrossRef]
32. Islamoglu, T.; Atilgan, A.; Moon, S.-Y.; Peterson, G.W.; DeCoste, J.B.; Hall, M.; Hupp, J.T.; Farha, O.K. Cerium (IV) vs zirconium (IV) based metal–organic frameworks for detoxification of a nerve agent. *Chem. Mater.* **2017**, *29*, 2672–2675. [CrossRef]

33. Vo, T.K.; Le, V.N.; Yoo, K.S.; Song, M.; Kim, D.; Kim, J. Facile synthesis of UiO-66 (Zr) using a microwave-assisted continuous tubular reactor and its application for toluene adsorption. *Cryst. Growth Des.* **2019**, *19*, 4949–4956. [CrossRef]
34. Chen, J.; Shen, K.; Li, Y. Greening the processes of metal–organic framework synthesis and their use in sustainable catalysis. *ChemSusChem* **2017**, *10*, 3165–3187. [CrossRef] [PubMed]
35. Yassin, J.M.; Taddesse, A.M.; Sánchez-Sánchez, M. Sustainable synthesis of semicrystalline Zr-BDC MOF and heterostructural Ag_3PO_4/Zr-BDC/g-C_3N_4 composite for photocatalytic dye degradation. *Catal. Today* **2022**, *390*, 162–175. [CrossRef]
36. Pakamorė, I.; Rousseau, J.; Rousseau, C.; Monflier, E.; Szilágyi, P.Á. An ambient-temperature aqueous synthesis of zirconium-based metal–organic frameworks. *Green Chem.* **2018**, *20*, 5292–5298. [CrossRef]
37. Assi, H.; Mouchaham, G.; Steunou, N.; Devic, T.; Serre, C. Titanium coordination compounds: From discrete metal complexes to metal–organic frameworks. *Chem. Soc. Rev.* **2017**, *46*, 3431–3452. [CrossRef]
38. Getachew, N.; Chebude, Y.; Diaz, I.; Sanchez-Sanchez, M. Room temperature synthesis of metal organic framework MOF-2. *J. Porous Mater.* **2014**, *21*, 769–773. [CrossRef]
39. Díaz-García, M.; Mayoral, A.; Diaz, I.; Sanchez-Sanchez, M. Nanoscaled M-MOF-74 materials prepared at room temperature. *Cryst. Growth Des.* **2014**, *14*, 2479–2487. [CrossRef]
40. Huang, Y.-H.; Lo, W.-S.; Kuo, Y.-W.; Chen, W.-J.; Lin, C.-H.; Shieh, F.-K. Green and rapid synthesis of zirconium metal–organic frameworks via mechanochemistry: UiO-66 analog nanocrystals obtained in one hundred seconds. *Chem. Commun.* **2017**, *53*, 5818–5821. [CrossRef]
41. He, T.; Xu, X.; Ni, B.; Wang, H.; Long, Y.; Hu, W.; Wang, X. Fast and scalable synthesis of uniform zirconium-, hafnium-based metal–organic framework nanocrystals. *Nanoscale* **2017**, *9*, 19209–19215. [CrossRef] [PubMed]
42. Taddei, M.; Dümbgen, K.C.; van Bokhoven, J.A.; Ranocchiari, M. Aging of the reaction mixture as a tool to modulate the crystallite size of UiO-66 into the low nanometer range. *Chem. Commun.* **2016**, *52*, 6411–6414. [CrossRef]
43. Botas, J.A.; Calleja, G.; Sanchez-Sanchez, M.; Orcajo, M.G. Effect of Zn/Co ratio in MOF-74 type materials containing exposed metal sites on their hydrogen adsorption behaviour and on their band gap energy. *Int. J. Hydrogen Energy.* **2011**, *36*, 10834–10844. [CrossRef]
44. Zeng, L.; Guo, X.; He, C.; Duan, C. Metal–organic frameworks: Versatile materials for heterogeneous photocatalysis. *ACS Catal.* **2016**, *6*, 7935–7947. [CrossRef]
45. Belousov, A.S.; Fukina, D.G.; Koryagin, A.V. Metal–organic framework-based heterojunction photocatalysts for organic pollutant degradation: Design, construction, and performances. *J. Chem. Technol. Biotechnol.* **2022**, *97*, 2675–2693. [CrossRef]
46. Alvaro, M.; Carbonell, E.; Ferrer, B.; Llabrés i Xamena, F.X.; Garcia, H. Semiconductor behavior of a metal-organic framework (MOF). *Chem. Eur. J.* **2007**, *13*, 5106–5112. [CrossRef]
47. Qiu, J.; Zhang, X.; Feng, Y.; Zhang, X.; Wang, H.; Yao, J. Modified metal-organic frameworks as photocatalysts. *Appl. Catal. B Environ.* **2018**, *231*, 317–342. [CrossRef]
48. Wen, Y.; Zhang, P.; Sharma, V.K.; Ma, X.; Zhou, H.-C. Metal-organic frameworks for environmental applications. *Cell Reports Phys. Sci.* **2021**, *2*, 100348. [CrossRef]
49. Liu, H.; Cheng, M.; Liu, Y.; Zhang, G.; Li, L.; Du, L.; Li, B.; Xiao, S.; Wang, G.; Yang, X. Modified UiO-66 as photocatalysts for boosting the carbon-neutral energy cycle and solving environmental remediation issues. *Coord. Chem. Rev.* **2022**, *458*, 214428. [CrossRef]
50. Kebede, T.; Taddesse, A.M.; Geresu, G.; Diaz, I.; Yassin, J.M. Boosted photocatalytic and antibacterial activities of polyaniline supported tandem nn ternary CdS-ZnO-Ag_3PO_4 composite under visible light irradiation. *J. Environ. Chem. Eng.* **2023**, *11*, 110338. [CrossRef]
51. Melillo, A.; Cabrero-Antonino, M.; Navalón, S.; Álvaro, M.; Ferrer, B.; García, H. Enhancing visible-light photocatalytic activity for overall water splitting in UiO-66 by controlling metal node composition. *Appl. Catal. B Environ.* **2020**, *278*, 119345. [CrossRef]
52. He, Y.; Li, C.; Chen, X.-B.; Shi, Z.; Feng, S. Visible-light-responsive UiO-66 (Zr) with defects efficiently promoting photocatalytic CO_2 reduction. *ACS Appl. Mater. Interfaces* **2022**, *14*, 28977–28984. [CrossRef] [PubMed]
53. Zhao, D.; Cai, C. Cerium-based UiO-66 metal-organic framework for synergistic dye adsorption and photodegradation: A discussion of the mechanism. *Dyes Pigm.* **2021**, *185*, 108957. [CrossRef]
54. Bibi, R.; Shen, Q.; Wei, L.; Hao, D.; Li, N.; Zhou, J. Hybrid BiOBr/UiO-66-NH_2 composite with enhanced visible-light driven photocatalytic activity toward RhB dye degradation. *RSC Adv.* **2018**, *8*, 2048–2058. [CrossRef] [PubMed]
55. Karadeniz, B.; Howarth, A.J.; Stolar, T.; Islamoglu, T.; Dejanović, I.; Tireli, M.; Wasson, M.C.; Moon, S.-Y.; Farha, O.K.; Friščić, T. Benign by design: Green and scalable synthesis of zirconium UiO-metal–organic frameworks by water-assisted mechanochemistry. *ACS Sustain. Chem. Eng.* **2018**, *6*, 15841–15849. [CrossRef]
56. Gan, C.; Xu, C.; Wang, H.; Zhang, N.; Zhang, J.; Fang, Y. Facile synthesis of rGO@ In_2S_3@ UiO-66 ternary composite with enhanced visible-light photodegradation activity for methyl orange. *J. Photochem. Photobiol. A* **2019**, *384*, 112025. [CrossRef]
57. Wang, X.; Sun, J.; Lin, H.; Chang, Z.; Wang, X.; Liu, G. A series of Anderson-type polyoxometalate-based metal–organic complexes: Their pH-dependent electrochemical behaviour, and as electrocatalysts and photocatalysts. *Dalton Trans.* **2016**, *45*, 12465–12478. [CrossRef]
58. Chen, J.; Chao, F.; Ma, X.; Zhu, Q.; Jiang, J.; Ren, J.; Guo, Y.; Lou, Y. Synthesis of flower-like CuS/UiO-66 composites with enhanced visible-light photocatalytic performance. *Inorg. Chem. Commun.* **2019**, *104*, 223–228. [CrossRef]

59. Yassin, J.M.; Taddesse, A.M.; Sánchez-Sánchez, M. Sustainable synthesis of a new semiamorphous Ti-BDC MOF material and the photocatalytic performance of its ternary composites with Ag_3PO_4 and g-C_3N_4. *Appl. Surf. Sci.* **2022**, *578*, 151996. [CrossRef]
60. Taddesse, A.M.; Bekele, T.; Diaz, I.; Adgo, A. Polyaniline supported CdS/CeO_2/Ag_3PO_4 nanocomposite: An "AB" type tandem nn heterojunctions with enhanced photocatalytic activity. *J. Photochem. Photobiol. A* **2021**, *406*, 113005. [CrossRef]
61. Gligorovski, S.; Strekowski, R.; Barbati, S.; Vione, D. Environmental implications of hydroxyl radicals (•OH). *Chem. Rev.* **2015**, *115*, 13051–13092. [CrossRef] [PubMed]
62. Sofi, F.A.; Majid, K. Enhancement of the photocatalytic performance and thermal stability of an iron based metal–organic-framework functionalised by Ag/Ag_3PO_4. *Mater. Chem. Front.* **2018**, *2*, 942–951. [CrossRef]
63. Bard, A.; Faulkner, L. *Electrochemical Methods: Fundamentals an d Applications*, 2nd ed.; Wiley: New York, NY, USA, 2001.
64. Chen, N.; Xia, J.; Li, L.; Lv, Q.; Zhao, K.; Ahmad, M.; Xiao, Z.; Wang, S.; Ye, F.; Zhang, Q. Comprehensive enhancement of photocatalytic H_2O_2 generation and antibacterial efficacy on carbon nitride through a straightforward polydopamine coating strategy. *Surf. Interfaces* **2025**, *56*, 105566. [CrossRef]
65. Fumanal, M.; Ortega-Guerrero, A.; Jablonka, K.M.; Smit, B.; Tavernelli, I. Charge Separation and Charge Carrier Mobility in Photocatalytic Metal-Organic Frameworks. *Adv. Funct. Mater.* **2020**, *30*, 2003792. [CrossRef]
66. Wu, X.-P.; Gagliardi, L.; Truhlar, D.G. Cerium metal–organic framework for photocatalysis. *J. Am. Chem. Soc.* **2018**, *140*, 7904–7912. [CrossRef] [PubMed]
67. Wen, Y.; Feng, M.; Zhang, P.; Zhou, H.-C.; Sharma, V.K.; Ma, X. Metal organic frameworks (MOFs) as photocatalysts for the degradation of agricultural pollutants in water. *ACS EST Eng.* **2021**, *1*, 804–826. [CrossRef]
68. Wang, C.-C.; Li, J.-R.; Lv, X.-L.; Zhang, Y.-Q.; Guo, G. Photocatalytic organic pollutants degradation in metal–organic frameworks. *Energy Environ. Sci.* **2014**, *7*, 2831–2867. [CrossRef]
69. Katsenis, A.D.; Puškarić, A.; Štrukil, V.; Mottillo, C.; Julien, P.A.; Užarević, K.; Pham, M.-H.; Do, T.-O.; Kimber, S.A.; Lazić, P. In situ X-ray diffraction monitoring of a mechanochemical reaction reveals a unique topology metal-organic framework. *Nat. Commun.* **2015**, *6*, 1–8. [CrossRef]
70. Užarević, K.; Wang, T.C.; Moon, S.-Y.; Fidelli, A.M.; Hupp, J.T.; Farha, O.K.; Friščić, T. Mechanochemical and solvent-free assembly of zirconium-based metal–organic frameworks. *Chem. Commun.* **2016**, *52*, 2133–2136. [CrossRef]
71. Julien, P.A.; Mottillo, C.; Friščić, T. Metal–organic frameworks meet scalable and sustainable synthesis. *Green Chem.* **2017**, *19*, 2729–2747. [CrossRef]
72. Lee, J.; Farha, O.K.; Roberts, J.; Scheidt, K.A.; Nguyen, S.T.; Hupp, J.T. Metal–organic framework materials as catalysts. *Chem. Soc. Rev.* **2009**, *38*, 1450–1459. [CrossRef]
73. Yaghi, O.M.; O'Keeffe, M.; Ockwig, N.W.; Chae, H.K.; Eddaoudi, M.; Kim, J. Reticular synthesis and the design of new materials. *Nature* **2003**, *423*, 705–714. [CrossRef] [PubMed]
74. Ploskonka, A.M.; Marzen, S.E.; DeCoste, J.B. Facile synthesis and direct activation of zirconium based metal–organic frameworks from acetone. *Ind. Eng. Chem. Res.* **2017**, *56*, 1478–1484. [CrossRef]
75. Huerta-Flores, A.M.; Sánchez-Martínez, D.; del Rocío Hernández-Romero, M.; Zarazúa-Morín, M.E.; Torres-Martínez, L.M. Visible-light-driven $BaBiO_3$ perovskite photocatalysts: Effect of physicochemical properties on the photoactivity towards water splitting and the removal of rhodamine B from aqueous systems. *J. Photochem. Photobiol. A* **2019**, *368*, 70–77. [CrossRef]
76. Huang, J.; Zhang, X.; Song, H.; Chen, C.; Han, F.; Wen, C. Protonated graphitic carbon nitride coated metal-organic frameworks with enhanced visible-light photocatalytic activity for contaminants degradation. *Appl. Surf. Sci.* **2018**, *441*, 85–98. [CrossRef]
77. Araya, T.; Jia, M.; Yang, J.; Zhao, P.; Cai, K.; Ma, W.; Huang, Y. Resin modified MIL-53 (Fe) MOF for improvement of photocatalytic performance. *Appl. Catal. B Environ.* **2017**, *203*, 768–777. [CrossRef]
78. Gayathri, K.; Vinothkumar, K.; Teja, Y.; Al-Shehri, B.M.; Selvaraj, M.; Sakar, M.; Balakrishna, R.G. Ligand-mediated band structure engineering and physiochemical properties of UiO-66 (Zr) metal-organic frameworks (MOFs) for solar-driven degradation of dye molecules. *Colloids Surf. APhysicochem. Eng. Asp.* **2022**, *653*, 129992. [CrossRef]
79. Mu, X.; Jiang, J.; Chao, F.; Lou, Y.; Chen, J. Ligand modification of UiO-66 with an unusual visible light photocatalytic behavior for RhB degradation. *Dalton Trans.* **2018**, *47*, 1895–1902. [CrossRef] [PubMed]
80. Sha, Z.; Wu, J. Enhanced visible-light photocatalytic performance of BiOBr/UiO-66 (Zr) composite for dye degradation with the assistance of UiO-66. *RSC Adv.* **2015**, *5*, 39592–39600. [CrossRef]
81. Zhang, F.; Cheng, W.; Yu, Z.; Ge, S.; Shao, Q.; Pan, D.; Liu, B.; Wang, X.; Guo, Z. Microwave hydrothermally synthesized WO_3/UiO-66 nanocomposites toward enhanced photocatalytic degradation of rhodamine B. *Adv. Compos. Hybrid Mater.* **2021**, *4*, 1330–1342. [CrossRef]

Disclaimer/Publisher's Note: The statements, opinions and data contained in all publications are solely those of the individual author(s) and contributor(s) and not of MDPI and/or the editor(s). MDPI and/or the editor(s) disclaim responsibility for any injury to people or property resulting from any ideas, methods, instructions or products referred to in the content.